Unraveling the topology of ZrTe$_5$ by changing temperature

Bartomeu Monserrat[*]

Cavendish Laboratory, University of Cambridge, J. J. Thomson Avenue, Cambridge CB3 0HE, United Kingdom

Awadhesh Narayan [†]

Solid State and Structural Chemistry Unit, Indian Institute of Science, Bangalore 560012, India

We study the effects of temperature on the topological nature of ZrTe$_5$, which sits near the phase boundary between strong and weak topological insulating orders. Using first-principles calculations, we show that the band gap and the topological indices of ZrTe$_5$ are extremely sensitive to thermal expansion and that the electron-phonon interaction accounts for more than a third of the total temperature-dependent effects in ZrTe$_5$. We find that the temperature dependence of the band gap has an opposite sign in the strong and weak topological insulator phases. Based on this insight, we propose a robust and unambiguous method to determine the topological nature of any given sample of ZrTe$_5$: If the band gap decreases with temperature it is a strong topological insulator, and if it increases with temperature it is a weak topological insulator. An analogous strategy is expected to be generally applicable to other materials and to become particularly important in the vicinity of topological phase boundaries where other methods provide ambiguous results.

I. INTRODUCTION

Topological insulators (TIs) and semimetals have become an important field of condensed matter over the past decade. TIs feature gapless surface states with spin-momentum locking that could be potentially useful for applications in spintronics and quantum computing [1,2]. More recently, their semimetallic counterparts, which include Dirac and Weyl semimetals and various flavors of nodal semimetals, have gained widespread interest [3].

An intriguing addition to the family of topological matter was made by Weng and coauthors, who proposed monolayers of transition-metal pentatellurides ZrTe$_5$ and HfTe$_5$ as large-gap quantum spin Hall insulators [4]. This prediction has sparked intense experimental and theoretical activity on this material system, not only in the monolayer form but also in the bulk. Additionally, ZrTe$_5$ has proved a fertile ground for the discovery of a number of exciting properties: chiral magnetic effect [5], log-periodic quantum oscillations [6], three-dimensional quantum Hall effect [7], and quantized thermoelectric Hall conductivity [8], to list just a few.

Despite this broad-ranging interest, the topological nature of *bulk* ZrTe$_5$ has not been unambiguously identified and has led to considerable debate. Using angle-resolved photoemission spectroscopy (ARPES), Manzoni and coworkers have

characterized ZrTe$_5$ as a strong TI [9]. Other ARPES measurements show a weak TI phase [10–12], which is also supported by scanning tunneling microscopy [13,14] and Shubnikov–de Haas oscillations [15]. Other experiments based on magnetotransport [5,16,17] and infrared spectroscopy [18,19] instead point to a Dirac semimetal phase. Yet other experiments using infrared spectroscopy observe a temperature-induced transition from a strong to a weak TI mediated by a Dirac semimetal [20]. An associated debate is that surrounding the dimensionality of the proposed Dirac cone in ZrTe$_5$ and whether it is gapped or gapless [12,19,21–26]. Many of these contradicting experimental results are supported by first-principles calculations, which raises the question of their reliability and predictive power.

In this contribution, we study the effects of temperature on the topological nature of ZrTe$_5$. We demonstrate that the band gap as well as the topological indices of this material are extremely sensitive to the volume and therefore to thermal expansion. Additionally, we calculate the change in the band gap of ZrTe$_5$ arising from electron-phonon coupling, which accounts for more than a third of the total temperature-dependent effects. We find that both volume and electron-phonon coupling corrections to the band gap have an opposite sign in the strong and weak TI regimes. Based on our results, we propose that monitoring the temperature dependence of the band gap provides an unambiguous way to determine the topological nature of any given sample of ZrTe$_5$, which may be more generally applicable to materials close to topological phase boundaries.

---

[*]bm418@cam.ac.uk

[†]awadhesh@iisc.ac.in

II. METHODS

We use first-principles methods based on density functional theory (DFT) [27,28] as implemented in the VASP
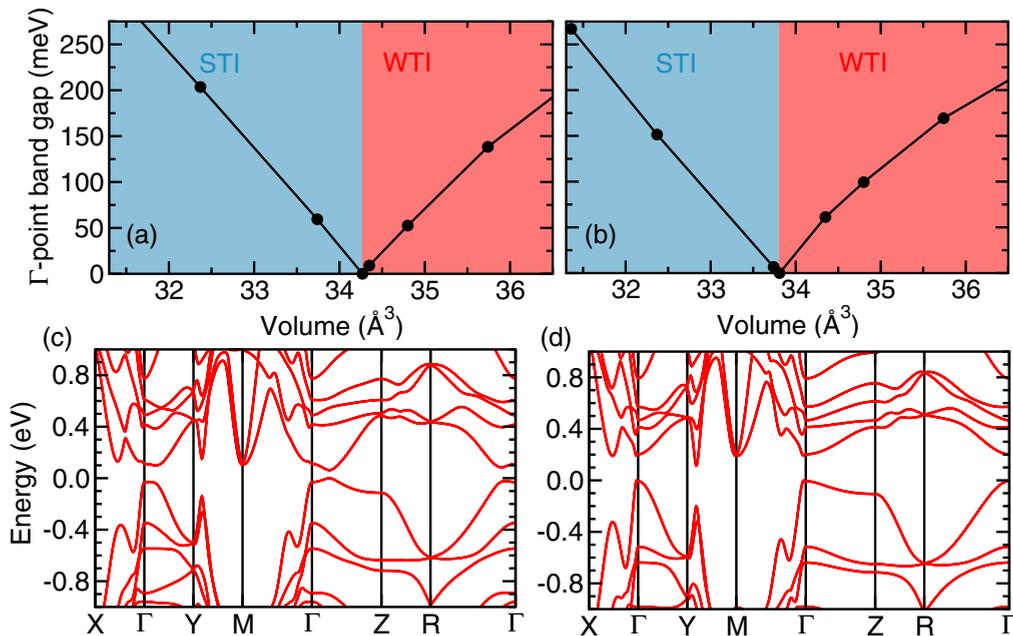
FIG. 1. Band gaps and band structures with volume. Band gap at the Γ point with increasing volume using (a) PBE and (b) HSE functionals. The shaded blue and red regions correspond to a strong topological insulator (STI) and a weak topological insulator (WTI) respectively. For both functionals, the band gap first decreases with increasing volume, vanishing at the critical value marking a topological phase transition. The gap then reopens with further increase in volume beyond the critical value. Representative band structures in (c) strong and (d) weak TI regimes.

code [29–32] within the projector augmented-wave formalism [33,34]. Based on convergence tests, we use an energy cutoff of 500 eV and a Brillouin zone (BZ) Monkhorst-Pack [35] **k**-point grid of size $8 \times 8 \times 4$ for primitive cell calculations, and commensurate grids for supercell calculations. We describe the exchange-correlation functional with the generalized gradient approximation of Perdew-Burke-Ernzerhof (PBE) [36] and also with the hybrid Heyd-Scuseria-Ernzerhof (HSE) functional [37,38]. The spin-orbit interaction is included as a perturbation to the scalar relativistic Hamiltonian, the so-called second variational method [39].

Based on our first-principles results, we construct a Wannier function based tight-binding model using the WANNIER90 code [40]. We include the Zr $4d$ and Te $5p$ orbitals in the model. We then calculated the topological invariants for different structures using the WANNIERTOOLS package [41].

The vibrational calculations are performed using the finite displacement method [42] in conjunction with nondiagonal supercells [43]. The matrix of force constants is explicitly calculated on a coarse $4 \times 4 \times 4$ **q**-point grid, and then the dynamical matrix is obtained on a finer grid to calculate phonon dispersions. We note that the phonon calculations are very sensitive to the electronic BZ sampling grid. We perform the electron-phonon coupling calculations on a grid of $2 \times 2 \times 1$ **q** points.

III. RESULTS AND DISCUSSION

Temperature impacts the electronic structure and topology of materials through two main contributions, thermal expansion, and electron-phonon coupling [44–51]. Using our first-principles approach, we are able to disentangle these two

effects and look at their individual contributions. We note that electronic temperature can also play a role, but only very close to the transition itself [52], and therefore we neglect this contribution in our calculations.

We find that both the band gap and the band topology of ZrTe$_5$ are extremely sensitive to the volume of the unit cell, and therefore to thermal expansion. Three-dimensional TIs are characterized by four indices $(\nu_0; \nu_1\nu_2\nu_3)$ [1]. Based on the value of ν_0, they can be classified into strong $(\nu_0 = 1)$ and weak $(\nu_0 = 0)$ TIs. At the relaxed PBE volume, we find ZrTe$_5$ to be a weak TI with the topological indices (0; 110). On the other hand, for the experimentally reported volumes at 10 and 300 K [53], we find a strong TI phase in both cases. The band gap at the BZ center (Γ) with increasing volume using the PBE functional is shown in Fig. 1(a). We find that, starting from small volumes, the band gap decreases with increasing volume in the strong TI phase. The gap vanishes at a critical volume, at which ZrTe$_5$ is a Dirac semimetal. The reopening of the band gap on further increase of the volume signals a topological phase transition into a weak TI. In the weak TI phase, the band gap increases with increasing volume, a trend opposite to the case of the strong topological insulator phase. We also calculate the band structure and band topology using the HSE functional, which is often more reliable to estimate band gaps. The Γ-point band gap as a function of volume obtained with HSE is presented in Fig. 1(b). We find a similar behavior of the band gap as a function of volume as in the case of PBE. While the critical value of volume at which the topological phase transition occurs is different by $\approx 1.3\%$ using PBE and HSE, the trend of decreasing gap with increasing volume in the strong TI phase and the opposite behavior in the weak TI regime are robust to the choice of theory.
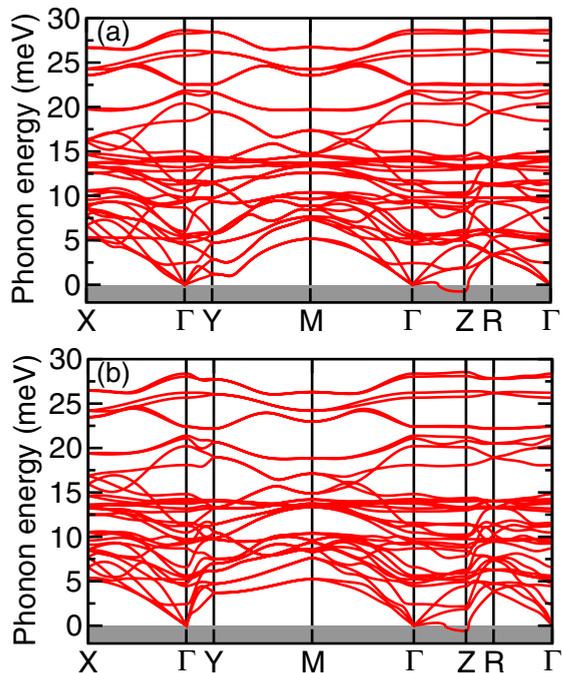
FIG. 2. Phonon spectra. Phonon dispersions (a) without spin-orbit coupling and (b) with spin-orbit coupling along the high symmetry directions. Note the presence of an imaginary phonon frequency at Z in both cases.

We note that our results are consistent with recent theoretical studies discussing the effect of volume on the band structure of ZrTe$_5$ [4,54]. However, to fully capture temperature-dependent material properties, the electron-phonon interaction also needs to be considered. As we will show next, these electron-phonon coupling effects are substantial and including them is essential for a complete understanding of the temperature dependence of the topological nature of ZrTe$_5$.

The phonon dispersion of ZrTe$_5$ is shown in Fig. 2 along a high symmetry path in the BZ obtained with SEEK-PATH [55]. The top diagram shows the results from calculations performed without the inclusion of spin-orbit coupling, while the bottom diagram shows the corresponding results including spin-orbit coupling. The dispersions exhibit some differences, most prominently in the low-energy region along the path Γ-Y-M, where the phonons calculated including spin-orbit coupling have higher energies than those calculated without. Importantly, both dispersion curves exhibit an imaginary phonon mode at the Z point, which indicates that the *Cmcm* structure of ZrTe$_5$ is not dynamically stable within the harmonic approximation and that a lower energy structure of ZrTe$_5$ exists. Indeed, by distorting the *Cmcm* structure along the imaginary phonon mode at Z and relaxing to the local minimum, we obtain a structure of *Pnnm* symmetry which is 0.7 meV per formula unit lower in energy than the initial structure. This result is at odds with experiments, which invariably report the higher symmetry *Cmcm* structure for ZrTe$_5$ [53,56–58].

Figure 3 shows the potential energy surface V_{ANH} of the *Cmcm* structure of ZrTe$_5$ along the imaginary phonon mode
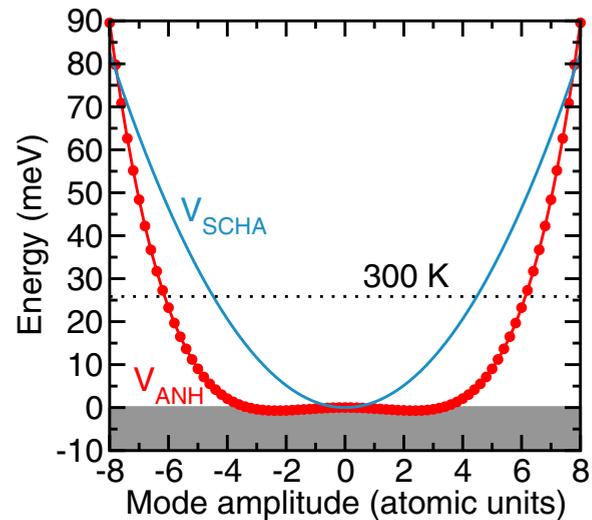

FIG. 3. Harmonic vs anharmonic approximations. Energy as a function of the amplitude of the imaginary phonon mode. The red circles denote the anharmonic energy profile, which shows a shallow double well. The blue line is the self-consistent harmonic approximation, exhibiting a single minimum at zero amplitude. The black dashed line denotes the energy at 300 K.

at Z. This diagram shows that a distortion along this mode leads to an anharmonic double-well potential. However, the energy scale of this anharmonic distortion is small compared to the thermal energy scale, which is 25.9 meV at 300 K (dotted black line in Fig. 3). This suggests that anharmonic lattice dynamics might stabilize the experimentally observed *Cmcm* structure of ZrTe$_5$. To explore this possibility, we limit our analysis to the anharmonic mode at Z and use the self-consistent harmonic approximation (SCHA) [59], which determines the effective harmonic free energy at some fixed temperature by including anharmonic terms in the total energy static potential. Consider a quartic anharmonic potential,

$$V_{ANH} = \tfrac{1}{2}\omega^2 u^2 + \tfrac{1}{4}\lambda u^4, \qquad (1)$$

where $\omega^2 < 0$ for the unstable mode at Z. The self-consistent harmonic potential at inverse temperature β is then $V_{SCHA} = \tfrac{1}{2}\Omega^2 u^2$, where [60]

$$\Omega^2 = \omega^2 + \frac{3\lambda}{2\Omega}\coth\left(\frac{\beta\Omega}{2}\right). \qquad (2)$$

We fit Eq. (1) to the anharmonic potential energy surface shown in Fig. 3 to determine ω and λ. We then solve Eq. (2) using a Newton-Raphson method, and the resulting potential V_{SCHA} at 300 K is depicted in Fig. 3. This potential can be thought of as the free energy potential at 300 K, which exhibits a single well and therefore demonstrates that anharmonic thermal motion dynamically stabilizes the experimentally observed *Cmcm* structure of ZrTe$_5$. Repeating this analysis at 10 K also leads to a single-well free energy potential, indicating that even quantum zero-point motion is sufficient to stabilize the *Cmcm* structure of ZrTe$_5$.

We calculate the change in the band gap of ZrTe$_5$ at inverse temperature β arising from electron-phonon coupling by evaluating the expectation value of electronic eigenvalues

TABLE I. Band gap of ZrTe$_5$ at the Γ point. $E_{\text{PBE}}^{\text{gap}}$ and $E_{\text{HSE}}^{\text{gap}}$ are the static gaps using PBE and HSE functionals, respectively, and the correction due to electron-phonon coupling, calculated with the PBE functional, is denoted by $\Delta E_{\text{el-ph}}^{\text{gap}}$.

Temperature	Volume	Topological indices	$E_{\text{PBE}}^{\text{gap}}$ (meV)	$E_{\text{HSE}}^{\text{gap}}$ (meV)	$\Delta E_{\text{el-ph}}^{\text{gap}}$ (meV)
10 K	Experiment at 10 K [53]	STI (1; 110)	173	122	-16 ± 1
300 K	Experiment at 300 K [53]	STI (1; 110)	141	91	-33 ± 2
10 K	PBE	WTI (0; 110)	210	224	$+3 \pm 1$
300 K	PBE	WTI (0; 110)	210	224	$+11 \pm 2$

$\epsilon_{\mathbf{k}n}$, labeled by momentum $\mathbf{k}$ and band index n, with respect to the vibrational density:

$$\epsilon_{\mathbf{k}n}(\beta) = \int \prod_{\mathbf{q}\nu} du_{\mathbf{q}\nu} \epsilon_{\mathbf{k}n}(\{u_{\mathbf{q}\nu}\})|\phi_{\mathbf{q}\nu}(u_{\mathbf{q}\nu};\beta)|^2. \qquad (3)$$

Phonon modes are labeled by their momentum $\mathbf{q}$ and branch index ν, and the vibrational density is $|\phi_{\mathbf{q}\nu}(u_{\mathbf{q}\nu};\beta)|^2 = [2\pi\sigma_{\mathbf{q}\nu}^2(\beta)]^{-1/2}\exp[-u_{\mathbf{q}\nu}^2/2\sigma_{\mathbf{q}\nu}^2(\beta)]$ with $\sigma_{\mathbf{q}\nu}^2(\beta) = (1/2\omega_{\mathbf{q}\nu})\coth(\beta\omega_{\mathbf{q}\nu}/2)$. In this expression, we treat the anharmonic phonon mode at Z within the self-consistent harmonic approximation, while all other phonon modes are treated within the harmonic approximation. We evaluate Eq. (3) using stochastic integration accelerated with thermal lines [61] at 10 and 300 K. We perform calculations for ZrTe$_5$ structures corresponding to the experimental volumes at 10 and 300 K and also for a fully relaxed structure using the PBE functional. The first two structures correspond to the regime in which ZrTe$_5$ is a strong TI, while the latter to the regime in which it is a weak TI.

Table I shows the correction to the band gap at the Γ point of ZrTe$_5$ calculated from electron-phonon coupling. In the strong TI regime, the band gap correction is negative, while in the weak TI regime the band correction is positive. The sign change in these corrections across the strong-to-weak topological transition arises because of the associated band inversion at the Γ point. We also note that increasing temperature enhances the magnitude of the correction in both regimes. Comparing with other materials exhibiting topological order, the band gap change induced by electron-phonon coupling in ZrTe$_5$ has a similar magnitude to that of BiTeI [50] and β-PbO$_2$ [62], while it is weaker than that in the Bi$_2$Se$_3$ family of topological insulators [47] and that in the alloy BiTl(S$_{1-\delta}$Se$_\delta$)$_2$ [48].

A full picture of the temperature dependence of the band gap of ZrTe$_5$ emerges from combining the thermal expansion and electron-phonon coupling results. In the strong TI regime, both thermal expansion and electron-phonon coupling contribute to decreasing the Γ-point band gap with increasing temperature, pushing ZrTe$_5$ toward the Dirac semimetal phase. In the weak TI regime, both thermal expansion and electron-phonon coupling contribute to increasing the Γ-point band gap with increasing temperature, moving ZrTe$_5$ away from the Dirac semimetal phase. We also note that increasing temperature leads to the closure of the band gap of the material, with the formation of a hole pocket at the Γ point and an associated electron pocket elsewhere in the BZ. This temperature-dependent shift of the electronic bands is consistent with experimental reports [63] and has been connected to the resistivity anomaly in ZrTe$_5$ [5,16,17,64,65].

It has proved challenging to determine the topological nature of ZrTe$_5$. Experimentally, strong TI, weak TI, and Dirac semimetal phases have been proposed. It is possible that these reports are not inconsistent, with the differences arising, for example, from different growth conditions (see, for instance, supplementary material in Ref. [6]). Many of these experiments rely on support from first-principles calculations to extract the topological nature of ZrTe$_5$, which seems to suggest that these calculations can be used to support any desired outcome. As we have shown, the calculated topological order depends critically on the level of theory and on the volume of the structural models used. As a consequence, absolute comparisons are uncertain due to the many sensitive variables, and this might explain the contradicting reports found in the literature. To resolve this, we propose a reliable method to determine the topology of ZrTe$_5$ which does not rely on uncertain absolute values but instead on robust changes. Our results suggest an unambiguous way of determining the topological nature of any given sample of ZrTe$_5$: If the band gap decreases with temperature it is a strong TI, and if the band gap increases with temperature it is a weak TI. A similar observation was made for BiTeI, which also shows an opposite sign in the temperature dependence of its band gap on either side of a pressure-induced topological phase transition [50]. We therefore propose that using temperature-dependent changes in band gaps is a general and robust way to identify topological phases, especially in systems in the vicinity of topological phase boundaries where different experimental conditions might lead to distinct conclusions.

Our proposed model is consistent with available temperature-dependent experimental data. Zhang and coworkers performed temperature-dependent angle-resolved photoemission measurements of the band gap of ZrTe$_5$ around the Γ point [11]. They observe an increase of the gap with increasing temperature, which in our proposed model would imply that their sample is a weak TI. Indeed, the lack of topological surface states in the in-plane surface in their experiments is attributed to a weak TI bulk order [11]. Xu and coworkers performed a temperature-dependent infrared spectroscopy study of ZrTe$_5$ revealing a topological phase transition from a strong TI at low temperatures to a weak TI at high temperatures [20]. Their observations can be consistently explained by our calculations incorporating both volume and electron-phonon coupling effects. Furthermore, they observe that the band-gap decrease with temperature in the strong TI regime is stronger than the band-gap increase with temperature in the weak TI regime. In our calculations, the volume-induced changes in the band gap are similar in both regimes and therefore cannot capture this experimental observation. Importantly, the inclusion

of electron-phonon coupling in the model does explain the experimental observation, as the electron-phonon coupling contribution is significantly weaker in the weak TI regime (see Table I).

IV. SUMMARY

We have shown that the band topology of ZrTe$_5$ is extremely sensitive to volume and consequently to thermal expansion. We have also shown that the change in the band gap of ZrTe$_5$ due to electron-phonon coupling accounts for more than a third of the total temperature-dependent effects in this material. Overall, both thermal expansion and electron-phonon coupling corrections to the band gap have an opposite sign in the strong and weak TI phases of ZrTe$_5$, explaining the available temperature-dependent experimental data. Based on these insights, we proposed a robust and unambiguous way to determine the topological nature of any given sample of ZrTe$_5$ by monitoring the temperature dependence of the band gap. This approach may be generally applicable to materials in the vicinity of topological phase boundaries, where other methods fail, as exemplified by the experimental controversies surrounding ZrTe$_5$.

[1] M. Z. Hasan and C. L. Kane, Rev. Mod. Phys. **82**, 3045 (2010).

[2] X.-L. Qi and S.-C. Zhang, Rev. Mod. Phys. **83**, 1057 (2011).

[3] N. P. Armitage, E. J. Mele, and A. Vishwanath, Rev. Mod. Phys. **90**, 015001 (2018).

[4] H. Weng, X. Dai, and Z. Fang, Phys. Rev. X **4**, 011002 (2014).

[5] Q. Li, D. E. Kharzeev, C. Zhang, Y. Huang, I. Pletikosić, A. V. Fedorov, R. D. Zhong, J. A. Schneeloch, G. D. Gu, and T. Valla, Nat. Phys. **12**, 550 (2016).

[6] H. Wang, H. Liu, Y. Li, Y. Liu, J. Wang, J. Liu, J.-Y. Dai, Y. Wang, L. Li, J. Yan *et al.*, Sci. Adv. **4**, eaau5096 (2018).

[7] F. Tang, Y. Ren, P. Wang, R. Zhong, J. Schneeloch, S. A. Yang, K. Yang, P. A. Lee, G. Gu, Z. Qiao, and L. Zhang, Nature (London) **569**, 537 (2019).

[8] W. Zhang, P. Wang, B. Skinner, R. Bi, V. Kozii, C.-W. Cho, R. Zhong, J. Schneeloch, D. Yu, G. Gu, L. Fu, X. Wu, and L. Zhang, arXiv:1904.02157 (unpublished).

[9] G. Manzoni, L. Gragnaniello, G. Autès, T. Kuhn, A. Sterzi, F. Cilento, M. Zacchigna, V. Enenkel, I. Vobornik, L. Barba, F. Bisti, P. Bugnon, A. Magrez, V. N. Strocov, H. Berger, O. V. Yazyev, M. Fonin, F. Parmigiani, and A. Crepaldi, Phys. Rev. Lett. **117**, 237601 (2016).

[10] L. Moreschini, J. C. Johannsen, H. Berger, J. Denlinger, C. Jozwiak, E. Rotenberg, K. S. Kim, A. Bostwick, and M. Grioni, Phys. Rev. B **94**, 081101(R) (2016).

[11] Y. Zhang, C. Wang, L. Yu, G. Liu, A. Liang, J. Huang, S. Nie, X. Sun, Y. Zhang, B. Shen, J. Liu, H. Weng, L. Zhao, G. Chen, X. Jia, C. Hu, Y. Ding, W. Zhao, Q. Gao, C. Li, S. He, L. Zhao, F. Zhang, S. Zhang, F. Yang, Z. Wang, Q. Peng, X. Dai, Z. Fang, Z. Xu, C. Chen, and X. J. Zhou, Nat. Commun. **8**, 15512 (2017).

[12] H. Xiong, J. A. Sobota, S.-L. Yang, H. Soifer, A. Gauthier, M.-H. Lu, Y.-Y. Lv, S.-H. Yao, D. Lu, M. Hashimoto, P. S. Kirchmann, Y.-F. Chen, and Z.-X. Shen, Phys. Rev. B **95**, 195119 (2017).

[13] X.-B. Li, W.-K. Huang, Y.-Y. Lv, K.-W. Zhang, C.-L. Yang, B.-B. Zhang, Y. B. Chen, S.-H. Yao, J. Zhou, M.-H. Lu, L. Sheng, S.-C. Li, J.-F. Jia, Q.-K. Xue, Y.-F. Chen, and D.-Y. Xing, Phys. Rev. Lett. **116**, 176803 (2016).

[14] R. Wu, J.-Z. Ma, S.-M. Nie, L.-X. Zhao, X. Huang, J.-X. Yin, B.-B. Fu, P. Richard, G.-F. Chen, Z. Fang, X. Dai, H.-M. Weng, T. Qian, H. Ding, and S. H. Pan, Phys. Rev. X **6**, 021017 (2016).

[15] Y.-Y. Lv, B.-B. Zhang, X. Li, K.-W. Zhang, X.-B. Li, S.-H. Yao, Y. B. Chen, J. Zhou, S.-T. Zhang, M.-H. Lu, S.-C. Li, and Y.-F. Chen, Phys. Rev. B **97**, 115137 (2018).

[16] G. Zheng, J. Lu, X. Zhu, W. Ning, Y. Han, H. Zhang, J. Zhang, C. Xi, J. Yang, H. Du, K. Yang, Y. Zhang, and M. Tian, Phys. Rev. B **93**, 115414 (2016).

[17] Y. Liu, X. Yuan, C. Zhang, Z. Jin, A. Narayan, C. Luo, Z. Chen, L. Yang, J. Zou, X. Wu, S. Sanvito, Z. Xia, L. Li, Z. Wang, and F. Xiu, Nat. Commun. **7**, 12516 (2016).

[18] R. Y. Chen, S. J. Zhang, J. A. Schneeloch, C. Zhang, Q. Li, G. D. Gu, and N. L. Wang, Phys. Rev. B **92**, 075107 (2015).

[19] R. Y. Chen, Z. G. Chen, X.-Y. Song, J. A. Schneeloch, G. D. Gu, F. Wang, and N. L. Wang, Phys. Rev. Lett. **115**, 176404 (2015).

[20] B. Xu, L. X. Zhao, P. Marsik, E. Sheveleva, F. Lyzwa, Y. M. Dai, G. F. Chen, X. G. Qiu, and C. Bernhard, Phys. Rev. Lett. **121**, 187401 (2018).

[21] X. Yuan, C. Zhang, Y. Liu, A. Narayan, C. Song, S. Shen, X. Sui, J. Xu, H. Yu, Z. An, J. Zhao, S. Sanvito, H. Yan, and F. Xiu, NPG Asia Mater. **8**, e325 (2016).

[22] Z.-G. Chen, R. Y. Chen, R. D. Zhong, J. Schneeloch, C. Zhang, Y. Huang, F. Qu, R. Yu, Q. Li, G. D. Gu, and N. L. Wang, Proc. Natl. Acad. Sci. USA **114**, 816 (2017).

[23] A. Pariari and P. Mandal, Sci. Rep. **7**, 40327 (2017).

[24] Y. Jiang, Z. L. Dun, H. D. Zhou, Z. Lu, K.-W. Chen, S. Moon, T. Besara, T. M. Siegrist, R. E. Baumbach, D. Smirnov, and Z. Jiang, Phys. Rev. B **96**, 041101(R) (2017).

[25] J. L. Zhang, C. M. Wang, C. Y. Guo, X. D. Zhu, J. Y. Yang, Y. Q. Wang, Z. Qu, L. Pi, H. Z. Lu, and M. L. Tian, Phys. Rev. Lett. **123**, 196602 (2019).

[26] E. Martino, I. Crassee, G. Eguchi, D. Santos-Cottin, R. D. Zhong, G. D. Gu, H. Berger, Z. Rukelj, M. Orlita, C. C. Homes, and A. Akrap, Phys. Rev. Lett. **122**, 217402 (2019).

[27] P. Hohenberg and W. Kohn, Phys. Rev. **136**, B864 (1964).

[28] W. Kohn and L. J. Sham, Phys. Rev. **140**, A1133 (1965).

[29] G. Kresse and J. Hafner, Phys. Rev. B **47**, 558 (1993).

[30] G. Kresse and J. Hafner, Phys. Rev. B **49**, 14251 (1994).

[31] G. Kresse and J. Furthmüller, Comput. Mater. Sci. **6**, 15 (1996).

[32] G. Kresse and J. Furthmüller, Phys. Rev. B **54**, 11169 (1996).

[33] P. E. Blöchl, Phys. Rev. B **50**, 17953 (1994).

[34] G. Kresse and D. Joubert, Phys. Rev. B **59**, 1758 (1999).

[35] H. J. Monkhorst and J. D. Pack, Phys. Rev. B **13**, 5188 (1976).

[36] J. P. Perdew, K. Burke, and M. Ernzerhof, Phys. Rev. Lett. **77**, 3865 (1996).

[37] J. Paier, M. Marsman, K. Hummer, G. Kresse, I. C. Gerber, and J. G. Ángyán, J. Chem. Phys. **124**, 154709 (2006).

[38] J. Paier, M. Marsman, K. Hummer, G. Kresse, I. C. Gerber, and J. G. Ángyán, J. Chem. Phys. **125**, 249901 (2006).

[39] D. D. Koelling and B. N. Harmon, J. Phys. C **10**, 3107 (1977).

[40] A. A. Mostofi, J. R. Yates, Y.-S. Lee, I. Souza, D. Vanderbilt, and N. Marzari, Comput. Phys. Commun. **178**, 685 (2008).

[41] Q. Wu, S. Zhang, H.-F. Song, M. Troyer, and A. A. Soluyanov, Comput. Phys. Commun. **224**, 405 (2018).

[42] K. Kunc and R. M. Martin, Phys. Rev. Lett. **48**, 406 (1982).

[43] J. H. Lloyd-Williams and B. Monserrat, Phys. Rev. B **92**, 184301 (2015).

[44] I. Garate, Phys. Rev. Lett. **110**, 046402 (2013).

[45] K. Saha and I. Garate, Phys. Rev. B **89**, 205103 (2014).

[46] J. Kim and S.-H. Jhi, Phys. Rev. B **92**, 125142 (2015).

[47] B. Monserrat and D. Vanderbilt, Phys. Rev. Lett. **117**, 226801 (2016).

[48] G. Antonius and S. G. Louie, Phys. Rev. Lett. **117**, 246401 (2016).

[49] L.-L. Wang, N. H. Jo, Y. Wu, Q. S. Wu, A. Kaminski, P. C. Canfield, and D. D. Johnson, Phys. Rev. B **95**, 165114 (2017).

[50] B. Monserrat and D. Vanderbilt, Phys. Rev. Mater. **1**, 054201 (2017).

[51] M. M. Möller, G. A. Sawatzky, M. Franz, and M. Berciu, Nat. Commun. **8**, 2267 (2017).

[52] E. Trushin and A. Görling, Phys. Rev. Lett. **120**, 146401 (2018).

[53] H. Fjellvåg and A. Kjekshus, Solid State Commun. **60**, 91 (1986).

[54] Z. Fan, Q.-F. Liang, Y. Chen, S.-H. Yao, and J. Zhou, Sci. Rep. **7**, 45667 (2017).

[55] Y. Hinuma, G. Pizzi, Y. Kumagai, F. Oba, and I. Tanaka, Comput. Mater. Sci. **128**, 140 (2017).

[56] S. Furuseth, L. Brattås, and A. Kjekshus, Acta Chem. Scand. **27**, 2367 (1973).

[57] H. Sodeck, H. Mikler, and K. L. Komarek, Monatsh. Chem. **110**, 1 (1979).

[58] T. Sambongi, K. Biljakovic, A. Smontara, and L. Guemas, Synth. Met. **10**, 161 (1985).

[59] D. J. Hooton, Phil. Mag. Ser. 7 **46**, 422 (1955).

[60] D. He, J. Thingna, J.-S. Wang, and B. Li, Phys. Rev. B **94**, 155411 (2016).

[61] B. Monserrat, Phys. Rev. B **93**, 014302 (2016).

[62] B. Peng, I. Bravic, J. L. MacManus-Driscoll, and B. Monserrat, Phys. Rev. B **100**, 161101(R) (2019).

[63] G. Manzoni, A. Sterzi, A. Crepaldi, M. Diego, F. Cilento, M. Zacchigna, P. Bugnon, H. Berger, A. Magrez, M. Grioni, and F. Parmigiani, Phys. Rev. Lett. **115**, 207402 (2015).

[64] E. Skelton, T. Wieting, S. Wolf, W. Fuller, D. U. Gubser, T. Francavilla, and F. Levy, Solid State Commun. **42**, 1 (1982).

[65] N. L. Nair, P. T. Dumitrescu, S. Channa, S. M. Griffin, J. B. Neaton, A. C. Potter, and J. G. Analytis, Phys. Rev. B **97**, 041111(R) (2018).